

# The role of intra-atomic non-collinear magnetization density in weak ferromagnetism

Robert Laskowski and Gilles Santi

Department of Physics and Astronomy, University of Aarhus, DK-8000 Aarhus C, Denmark

(Dated: November 13, 2018)

We investigate the mechanism behind the breakdown of the compensation of large magnetic moments leading to weak ferromagnetism. For this we use first-principles calculations within density functional theory and we focus on the weak ferromagnetic compound  $\text{Mn}_3\text{Sn}$ . Our new implementation allows for an exact treatment of the spin-density matrix and non-collinearity. In order to gain some insight, our results are compared to the ones obtained by using the atomic moment approximation (AMA) and its role is discussed. We find that the appearance of the weak ferromagnetic moment in this compound originates not so much as an effect of spin-orbit coupling as suggested previously from AMA calculations, as from the non-collinearity of the Sn atom magnetization density. This is confirmed by non-collinear calculations in which the SOC effects are neglected.

Weak ferromagnetism is a phenomenon commonly characterized by a small net magnetic moment in a system of large localized moments nearly canceling each other. It has been known for more than 50 years and observed both in metallic and insulating materials (e.g.  $\alpha\text{-Fe}_2\text{O}_3$ , carbonates of Mn and Co,  $\text{NiF}_2$ ,  $\text{Mn}_3\text{Sn}$  or  $\text{Mn}_3\text{Ge}$ ). The earliest trial to devise a model Hamiltonian describing the mechanism behind it was put forward by Dzialoshinski [1] and was based on Landau's theory of second order phase transitions. Moriya presented a more rigorous derivation for magnetic insulators [2], extending Anderson's theory of superexchange to include spin-orbit coupling (SOC). Kataoka *et al.* refined this theory further and applied it to metals [3]. These models identify two types of interactions responsible for the appearance of weak ferromagnetism, i.e. the magnetocrystalline anisotropy and the antisymmetrical part of the anisotropic superexchange.

This problem has also been approached from the point of view of first-principles calculations within density functional theory (DFT). An early local spin density approximation (LSDA) calculation for  $\text{Mn}_3\text{Sn}$  within the atomic moment approximation (AMA), which neglected SOC, was however not able to resolve the weak ferromagnetic structure [4]. Subsequently, including SOC effects into the DFT Hamiltonian, Sandratskii and Kübler concluded that this is essential to the correct description of weak ferromagnetism [5, 6].

In this Letter, we use our newly developed method [7] that incorporates non-collinear effects into the all electron linearized augmented plane wave plus local orbital (L/APW+lo) WIEN2k code [8]. Our implementation is based on a mixed spinor basis set approach [9, 10]. In the interstitial region the basis functions are pure spinors given in a global spin coordinate frame, whereas, inside the atomic spheres, they are non-pure spinors given in the (local) sphere's spin coordinate frame with the quantization axis pointing along the sphere's average magnetization. One advantage of this method is that it allows the use of spin-polarized radial basis functions. In addition, we have extended the implementation of Kurz *et*

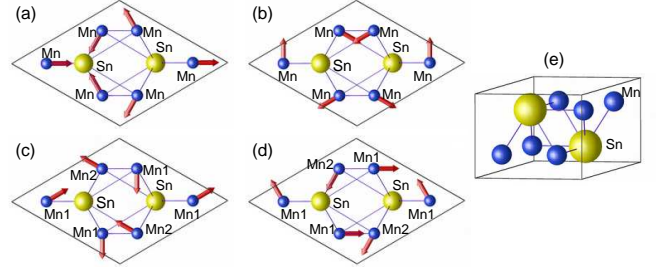


FIG. 1: Candidate magnetic structures for  $\text{Mn}_3\text{Sn}$  (a)–(d) and unit cell (e). (The 4 Mn1 atoms and the 2 Mn2 ones are not equivalent in structures (c) and (d)).

*al.* [10] described recently in order to treat the spins fully non-collinearly also inside the spheres. This means that the off-diagonal terms of the spin-potential matrix inside the atomic spheres are taken into account. The full spin-potential matrix is evaluated from the spin-density matrix using the methodology applied to interstitial charge [10]. The method uses the fact that the exchange potential is local and can be evaluated independently at each point of the unit cell. Because the standard LSDA formulation applies only to the collinear case (i.e. diagonal spin-density matrix) we rotate the spin-density matrix in spin-space to its diagonal form at each point in the unit cell independently. The diagonal potential matrix (at this point in space) is then evaluated in this “local” spin frame and rotated back into the original spin frame, leading to off-diagonal matrix elements. As the treatment of non-collinearity requires the “full” spin Hamiltonian, SOC [11] is naturally added to the scalar relativistic Hamiltonian in this first variational step. To demonstrate the importance of such an exact treatment of the spin-density matrix, we focus, in this paper, on the case of the weak ferromagnet  $\text{Mn}_3\text{Sn}$ .

The magnetic behavior of  $\text{Mn}_3\text{Sn}$  has been the subject of a number of experimental studies beginning from the early sixties. Weak ferromagnetism in this compound was first discovered by Yasukochi *et al.* [12] and Ohoyama [13]. According to several neutron diffraction measure-

ments [14, 15, 16, 17, 18, and references therein],  $\text{Mn}_3\text{Sn}$  displays a quite interesting temperature dependence of the magnetization which depends however on the stoichiometry (the structure can be stabilized only in the presence of some excess of Mn) and the thermal treatment. It can be characterized by three temperatures:  $T_N \approx 420$  K, at which weak ferromagnetism appears,  $T_1 \approx 150\text{--}270$  K, at which magnetization vanishes almost entirely (with the possible appearance of an incommensurate spin-spiral state), and  $T_2 \approx 50\text{--}100$  K, at which the magnetization increases again to reach its maximum value for  $T = 0$ . The chemical unit cell is of  $\text{DO}_{19}$  type, with hexagonal space group  $P6_3/mmc$ , and contains two formula units. It is composed of two layers of Mn atoms arranged in triangles, with an Sn atom on top of each triangle (Fig. 1). Only a limited number of magnetic structures are compatible with the  $\text{DO}_{19}$  type symmetry [4, 18]. Neutron diffraction data was compatible with two of them (structures (c) and (d) in Fig. 1), but could not discriminate between them [18]. Following Sandratskii and Kübler [5], we focus here on these two magnetic structures as well as the two additional ones which are symmetry equivalent when SOC is neglected and Sn atoms are assumed non-magnetic (structure (a) and (b) in Fig. 1).

One of the most important aspect we are going to discuss is the effect of the atomic moment approximation (AMA), which is widely used in non-collinear magnetic calculations, compared to the exact treatment of non-collinearity. We show here that the key role in producing the weak ferromagnetic moment in  $\text{Mn}_3\text{Sn}$  is not played by the SOC interaction as suggested by Sandratskii *et al.* [5, 6], but by the precise non-collinear magnetic density on the Sn atom which cannot be described within the AMA. In a way it is very surprising as the Sn atoms do not carry any magnetic moment on average.

All the calculations presented in this work were performed using the Perdew-Wang LSDA exchange-correlation potential [19]. We found no noticeable differences between test generalized gradient approximation (GGA) [20] calculations and LSDA ones. Note that, as GGA is not formulated for non-collinear spin-densities, we use the gradient of the norm of the magnetization density vector as the scalar magnetization density entering in the standard formulation. The details of the setting for the L/APW+lo calculations are as follows. The atomic sphere radii were set to 2.5 a.u. for both Mn and Sn atoms. The basis size was setup according to  $R_{\text{MT}}K_{\text{max}} = 6.9$  ( $R_{\text{MT}}$  is the smallest atomic sphere radius,  $K_{\text{max}}$  is a cutoff for the basis functions wave vector). Brillouin zone integrations were performed on a  $7 \times 7 \times 7$  mesh (which corresponds to 48 and 64 k-points in the irreducible wedge for structures (a), (b) and (c), (d) respectively (see Fig. 1)).

We have calculated the electronic structures and total energies of the four non-collinear magnetic structures

presented in Fig. 1. For this we used two approaches: (1) AMA, in which the off-diagonal part of the spin-density matrix inside the atomic spheres is ignored, and, (2) the exact treatment, where no shape approximation is imposed on the spin-density and spin-potential matrices. Moreover, each of these calculations has been run with and without taking into account SOC.

Sandraskii and Kübler [5] have already pointed out that symmetry analysis is very helpful in understanding the mechanism responsible for the advent of weak ferromagnetism in  $\text{Mn}_3\text{Sn}$ . Assuming the Sn atoms are non-magnetic, they showed that all four structures (Fig. 1) are equivalent by symmetry when SOC is neglected. Indeed, in the absence of SOC, the spin space can be freely globally rotated with respect to the real one. It must be noted however that any magnetization density on the Sn atom would break this equivalency irrespective of the inclusion of SOC effects. For example, the (a) and (b) structure in Fig. 1 appear to be symmetrically related by a pure  $90^\circ$  spin-rotation and identity in real space. However, this is not an allowed symmetry operation of the magnetic crystal structure as it would rotate the spin-density on the Sn site by  $90^\circ$  and there is no such four-fold symmetry axis on this atom (see Fig. 2). Similar arguments lead to the fact that the four structures are inequivalent.

It is clear that the magnetic structure is determined by moments localized on Mn atoms. Sn atoms are essentially non-magnetic in the sense that they do not carry any average spin moments. Nevertheless, their complicated intra-atomic magnetic structure (due to neighboring Mn atoms) has to be properly taken into account. We construct the magnetic symmetry group by using a two stage algorithm: (1) the symmetry group is determined solely on the basis of the localized Mn moments (assuming that the spin-density is identically zero within the Sn sites and are thus symmetrical with respect to any rotations in spin-space); (2) the quantization axes on the Sn atoms are determined in such a way that they preserve the symmetry operations that we have just found (using the singular value decomposition technique). As a result, the quantization axes of the two Sn atoms are along  $+c$  and  $-c$  directions for both structures (a) and (b), whereas they are in the  $(ab)$ -plane for structures (c) and (d) (i.e. parallel to the Mn2 atoms' moments in Fig. 1). The number of symmetry operations is decreased from 24 in the paramagnetic symmetry group to 12 for structures (a) and (b), and 8 for (c) and (d). All Mn atoms are equivalent in structures (a) and (b), and the triangular arrangement of their moments is univocally determined by symmetry. For structures (c) and (d) the six Mn atoms are split into two equivalency classes containing four Mn1 and two Mn2 atoms. The directions of the magnetic moments of Mn2 atoms are fixed by symmetry, whereas the moments of Mn1 atoms can be freely rotated in the  $(ab)$ -plane and have therefore to be optimized during self-consistency.

TABLE I: Total energies (in mRy) of structures (b), (c) and (d) relative to the energy of structure (a), and weak ferromagnetic (FM) spin and orbital (in parenthesis) moments per unit cell, calculated with different approximations. AMA stands for atomic moment approximation, “Full” stands for exact treatment of the spin-density, M1 means that Mn atoms are treated exactly and Sn ones within AMA, M2 means that Mn are treated within AMA and Sn exactly.

	Total energies [mRy]			FM moment [ $10^{-2}\mu_B$ ]	
	b	c	d	c	d
AMA	-0.02	-0.08	-0.08	0.9	0.3
AMA + SOC	-0.06	-0.42	-0.42	0.8 (0.07)	0.4 (-0.04)
Full	-0.01	-2.46	-2.53	6.7	1.3
Full + SOC	-0.01	-2.90	-2.98	7.5 (-0.15)	1.4 (0.27)
M1	-0.0	0.71	0.71	1.6	1.2
M1 + SOC	-0.09	0.13	0.13	1.5 (0.27)	1.5 (-0.23)
M2	0.027	-1.8	-1.76	1.6	1.3
M2 + SOC	0.52	-1.57	-1.59	1.5 (0.27)	1.8 (-0.24)

The results of our total energy calculations are presented in Table I. Our AMA and AMA+SOC calculations confirm the previous results of Sandratskii and Kübler [5]. Non-relativistic AMA total energies for all structures are found in an energy window which is less than 0.1 mRy wide. We ascribe the slight lifting of this degeneracy to the fact that, in LAPW, AMA cannot be applied to the interstitial region where the magnetization must be treated as a continuous field. SOC shifts down the total energies of structures (c) and (d) by about 0.4 mRy with respect to structure (a). The total spin and orbital moments calculated within AMA (which are zero for structures (a) and (b) due to symmetry) are two to three times larger for structure (c) than for structure (d). In both cases orbital contributions are about ten times smaller than the spin ones. In addition, the orbital moment is parallel or anti-parallel to the spin moment for structures (c) or (d) respectively.

The most important point we want to address here is the result of our full non-collinear calculations. They show that structures (c) and (d) have a lower energy (by about 2.5 – 3 mRy) than structures (a) and (b), irrespective of the inclusion of SOC effects. This is in clear opposition to previous conclusions concerning the essential role of SOC in the formation of the weak ferromagnetic moment in  $\text{Mn}_3\text{Sn}$  [5, 6]. As can be seen from Table I, the effect of spin-lattice coupling is much smaller than the effect of switching from AMA to an exact treatment of non-collinearity. Similarly to the AMA case, the SOC further decreases the total energies of structures (c) and (d) by about 0.4 mRy. Furthermore, as was the case with AMA, the weak ferromagnetic moments for the exact calculations are much bigger in the (c) magnetic configuration than in the (d) one, but are however about 5 – 10 times larger than their AMA counterparts. In addition, the orientation of the orbital moments changed sign relative to the spin moments. For completeness, we

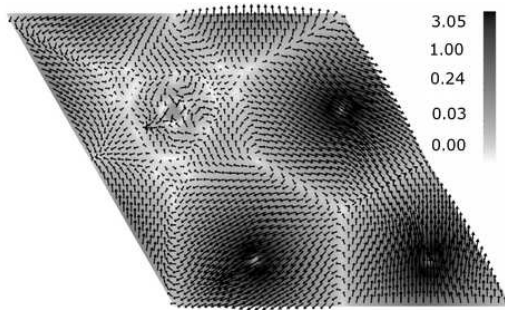


FIG. 2: Calculated spin density for structure (d) plotted in the (001) plane cutting three Mn and one Sn atoms [ $\mu_B/\text{a.u.}^3$ ], using the exact treatment of non-collinearity and SOC. An exponential scale is used in order to enhance the visibility of regions of low spin density.

want to add that the antiferromagnetic collinear structure with moments along  $c$  has a total energy higher by 34 mRy for AMA and 26 mRy for the exact calculation with respect to the energy of structure (a).

The fact that structures (c) and (d) are stabilized by the exact non-collinear treatment, irrespective of SOC effects, emphasizes the importance of the off-diagonal terms in the spin-density and potential matrices. In order to gain physical insight, we show a map of the magnetization density for the (d) configuration in Fig. 2. The relatively simple triangular magnetic structure on the Mn atoms polarizes the Sn atoms, resulting in a complicated and interesting magnetization density on the Sn atoms. It displays a symmetrical pattern leading to a total Sn moment of zero (integrated over the Muffin-Tin volume). The question of the importance of the non-collinearity of the small Sn atom spin density to the weak ferromagnetism of  $\text{Mn}_3\text{Sn}$  arises. To address this, we have carried out calculations in which the Mn and Sn atoms are treated within different levels of approximation. These results are presented in the bottom part of Table I, where M1 stands for Mn atoms treated exactly and Sn ones within AMA and M2 for the opposite. This shows that the M2 case captures the physics of the exact calculation (i.e. that the (c) and (d) configurations are stabilized with respect to the (a) and (b) ones) whereas the M1 makes the (c) and (d) structures less energetically favorable. This means that the intra-atomic non-collinearity of Sn atoms plays the essential role in stabilizing the (c) and (d) magnetic structures and, therefore, in the weak ferromagnetism of  $\text{Mn}_3\text{Sn}$ .

We now consider some atomic properties (see Table II) which could be used experimentally to discriminate between magnetic structures or levels of approximation. As could be expected from their average nature, the local atomic magnetic moments are practically the same for both AMA and exact treatment and for all structures. Similarly, the electrical field gradients (EFG) [21, 22]

TABLE II: Electric field gradients (EFG) in [ $10^{21}\text{V}/\text{m}^2$ ], total hyperfine fields (HFF) in kGauss, spin ( $M_s$ ) and orbital ( $M_{\text{orb}}$ ) moments for Mn and Sn atoms in  $\mu_B$ . All results include SOC effects. Values for the Mn2 atoms (where relevant) are in parentheses.

			a	b	c	d
$M_s$	Mn		3.03	3.03	3.03	3.03
	Sn		0	0	0	0
$M_{\text{orb}}$	Mn		0.04	0.04	0.03	0.03
	Sn		0	0	0.0015	0.0015
EFG	Mn	Full	-1.09	-1.11	-1.08 (-1.09)	-1.08 (-1.07)
	Mn	AMA	-1.05	-1.07	-1.03 (-1.04)	-1.04 (-1.03)
	Sn	Full	-2.12	-2.11	-2.29	-2.29
	Sn	AMA	-2.05	-2.05	-2.17	-2.17
HFF	Mn	Full	66.7	43.1	59.5 (41.2)	49.1 (62.5)
	Mn	AMA	60.2	38.9	53.6 (40.4)	44.5 (58.5)

depend neither on the level of approximation used in the calculations (AMA or exact), nor on the magnetic configuration (apart, perhaps, for the Sn atom between structures (a), (b) and (c), (d)). Calculated hyperfine fields (HFF) [23] turn out to be much more interesting. First, they depend on the methodology (AMA or exact) by about 10% and, second, they are sensitive to the magnetic configuration (Table II). They exhibit a 20% difference between the two inequivalent Mn atoms (bigger by about 20% on the 4 Mn1 atoms than on the 2 Mn2 ones for the (c) configuration and the opposite for the (d) one) which could be used to discriminate between magnetic configurations. This difference can be ascribed almost entirely on the so-called dipole term [23]. It must be noted that HFF are known to be underestimated by LDA by about 20%, but this affects the “contact term” [24] which does not depend on the details of the magnetic configuration and should therefore not influence this difference.

To conclude we have presented the results of our *ab-initio* calculations of the weak ferromagnet  $\text{Mn}_3\text{Sn}$ , emphasizing the importance of non-collinearity and the short-comings of the atomic moment approximation. The comparison between the AMA and exact non-collinear calculations shows that the AMA is appropriate for the description of atomic properties such as magnetic moments and electrical field gradients. However, the AMA leads to the erroneous conclusion that spin-lattice coupling is the sole and main mechanism leading to weak ferromagnetism in  $\text{Mn}_3\text{Sn}$ . Our exact treatment of non-collinearity shows that the weak ferromagnetic moment find its origin in the non-collinear intra-atomic magnetization density on the Sn atom. To some extent, the fact that such a small magnetization density (Fig. 2) drives a larger decrease in energy than spin-orbit coupling effects can be seen as surprising. The magnetic configuration (d) has the lowest energy, but by only 0.08 mRy with respect to configuration (c). It is therefore difficult to give a definite statement about the most stable magnetic state on

that basis. However, the total magnetic moment of  $0.017 \mu_B/\text{cell}$  (2 formula units per unit cell) for structure (d) is in much better agreement with the measured moment of  $0.01 \mu_B/\text{cell}$  [14] than the five times larger moment for structure (c). This suggests that magnetic structure (d) is realized by nature.

We are grateful to the “EXCITING” and “*f*-electron” European Research and Training Networks for providing financial support, and to the Danish Centre for Scientific Computing for computational resources.

- 
- [1] I. J. Dzialoshinski, Phys. Chem. Solids **4**, 241 (1958).
  - [2] T. Moriya, Phys. Rev. **120**, 91 (1960).
  - [3] M. Kataoka, O. Nakanishi, A. Yanase, and J. Kanamori, J. Phys. Soc. Jpn. **53**, 3624 (1984).
  - [4] J. Sticht, K. H. Höck, and J. Kübler, J. Phys. Condens. Matter. **1**, 8155 (1989).
  - [5] L. M. Sandratskii and J. Kübler, Phys. Rev. Lett. **76**, 4963 (1996).
  - [6] L. M. Sandratskii, Advances in Phys. **47**, 91 (1998).
  - [7] R. Laskowski, G. K. H. Madsen, P. Blaha, and K. Schwarz, Phys. Rev. B **69**, 140408(R) (2004).
  - [8] P. Blaha, K. Schwarz, G. K. H. Madsen, D. Kvasnicka, and J. Luitz, *WIEN2k, An Augmented Plane Wave Plus Local Orbitals Program for Calculating Crystal Properties. ISBN 3-9501031-1-2*, Vienna University of Technology, Austria (2001).
  - [9] H. Yamagami, Phys. Rev. B **61**, 6246 (2000).
  - [10] P. Kurz, F. Förster, L. Nordström, G. Bihlmayer, and S. Blügel, Phys. Rev. B **69**, 24415 (2004).
  - [11] A. H. MacDonald, W. E. Pickett, and D. D. Koelling, J. Phys. C: Solid St. Phys. **13**, 2675 (1980).
  - [12] K. Yasukocji, K. Kanematsu, and T. Ohoyama, J. Phys. Soc. Jpn **16**, 1123 (1961).
  - [13] T. Ohoyama, J. Phys. Soc. Jpn **16**, 1995 (1961).
  - [14] S. Tomiyoshi and Y. Yamaguchi, J. Phys. Soc. Jpn **51**, 2478 (1982).
  - [15] S. Tomiyoshi, S. Abe, Y. Yamaguchi, H. Yamaguchi, and H. Yamamoto, J. Magn. Magn. Mater **54-57**, 1001 (1986).
  - [16] S. Tomiyoshi, H. Yoshoda, H. Ohmori, T. Kaneko, and H. Yamamoto, J. Magn. Magn. Mater **70**, 247 (1987).
  - [17] H. Ohmori, S. Tomiyoshi, H. Yamaguchi, and H. Yamamoto, J. Magn. Magn. Mater **70**, 249 (1987).
  - [18] P. Brown, V. Nunez, F. Tasset, and P. Forsyth, J. B. nad Radhakrishna, J. Phys. Condens. Matter **2**, 9409 (1990).
  - [19] J. P. Perdew and Y. Wang, Phys. Rev. B **45**, 13244 (1992).
  - [20] J. P. Perdew, K. Burke, and M. Ernzerhof, Phys. Rev. Lett. **77**, 3865 (1996).
  - [21] P. Blaha, K. Schwarz, and P. H. Dederichs, Phys. Rev. B **37**, 2792 (1988).
  - [22] P. Blaha, K. Schwarz, W. Faber, and J. Luitz, Hyperfine Interact. **126**, 389 (2000).
  - [23] S. Blügel, H. Akai, R. Zeller, and P. H. Dederichs, Phys. Rev. B **35**, 3271 (1987).
  - [24] P. Novák, J. Kuneš, W. E. Pickett, W. Ku, and F. R. Wagner, Phys. Rev. B **67**, 140403(R) (2003).